Response of the Atlantic Ocean circulation to Greenland Ice Sheet melting in a strongly-eddying ocean model

W. Weijer,[1,2] M. E. Maltrud,[1] M. W. Hecht,[1] H. A. Dijkstra,[3] and M. A. Kliphuis[3]

Received 6 March 2012; revised 6 April 2012; accepted 9 April 2012; published 11 May 2012.

[1] The sensitivity of the Atlantic Meridional Overturning Circulation (AMOC) to high-latitude freshwater input is one of the key uncertainties in the climate system. Considering the importance of the AMOC for global heat transports, and the vulnerability of the Greenland Ice Sheet (GrIS) to global warming, assessing this sensitivity is critical for climate change projections. Here we present a unique set of computational experiments to investigate the adjustment of the AMOC to enhanced melt water from the GrIS under present-day conditions. For the first time, the response in a global, strongly-eddying ocean model is systematically compared to that of an ocean model typical of IPCC-class climate models. We find that the overall decline of the AMOC on decadal time scales is quantitatively similar (<10%) in the two configurations. Nonetheless, the transient response is significantly different, as the AMOC decline and reduction in wintertime convection is markedly more gradual and persistent in the strongly-eddying configuration. **Citation:** Weijer, W., M. E. Maltrud, M. W. Hecht, H. A. Dijkstra, and M. A. Kliphuis (2012), Response of the Atlantic Ocean circulation to Greenland Ice Sheet melting in a strongly-eddying ocean model, *Geophys. Res. Lett.*, *39*, L09606, doi:10.1029/2012GL051611.

1. Introduction

[2] Since Stommel's seminal paper [*Stommel*, 1961] many studies have shown that the Atlantic Meridional Overturning Circulation (AMOC) may be sensitive to changes in the freshwater balance of the northern North Atlantic [*Rooth*, 1982; *Maier-Reimer and Mikolajewicz*, 1989; *Rahmstorf*, 1995a]. Freshening of the surface waters in the Nordic and Labrador Seas inhibits deep convection and hence the production of North Atlantic Deep Water (NADW), which feeds the deep southward branch of the AMOC.

[3] One of the potential sources of freshwater that might affect the AMOC is enhanced freshwater discharge from the Greenland Ice Sheet (GrIS). It has become increasingly clear that the mass balance of the GrIS is negative [*Wu et al.*, 2010], and that the mass deficit has been increasing [*Velicogna*, 2009]: from a near-zero balance in the 1970s, estimates of the mass deficit of the GrIS have now reached values close to 300 Gt/yr [*Rignot et al.*, 2008; *Velicogna*, 2009]. Enhanced run-off and iceberg discharge are estimated to contribute in equal parts to this deficit [*van den Broeke et al.*, 2009], while increases in precipitation have partially offset these mass losses.

[4] The sensitivity of the AMOC with respect to freshwater fluxes has been studied using both Ocean General Circulation Models (OGCMs) and fully-coupled climate models. A popular procedure is the so-called "hosing" experiment, where an anomalous freshwater flux is applied over a broad swath of the subpolar North Atlantic [*Rahmstorf*, 1995a; *Stouffer et al.*, 2006]. This hosing prescription directly affects the mid-ocean areas where deep convection takes place (Nordic and Labrador Seas). In contrast, runoff from the GrIS occurs in a narrow strip around the coast of Greenland and an explicit mechanism is required to transport the freshwater to the deep convection sites. Although recent experiments with a low-resolution model suggest that the AMOC response is rather robust with respect to details of the freshwater distribution [*Kleinen et al.*, 2009], the relevance of this hosing prescription to the scenario of enhanced coastal runoff from Greenland in a strongly-eddying ocean has remained unclear.

[5] Another issue of resolution concerns the ability of the OGCM to represent the transports by western boundary currents and meso-scale eddies. Indeed, recent observations have changed our view of the AMOC from a relatively steady, coherent feature — famously depicted by *Broecker* [1991] as a conveyor belt, an image reinforced by the sluggish representation of the AMOC in early-generation OGCMs [*Drijfhout et al.*, 1996] — to a highly variable residual circulation of a strongly eddying fluid [*Cunningham et al.*, 2007], where few water parcels follow the traditional overturning pathways [*Brambilla and Talley*, 2006; *Bower et al.*, 2009; *Lozier*, 2010]. A recent study using an eddy-permitting (0.4° resolution) ocean model shows how narrow boundary currents around Greenland limit access of the freshwater anomalies to the deep convection sites [*Marsh et al.*, 2010]. Due to the short, 8-year duration of that experiment, however, no conclusion could be drawn on the longer-term response of the AMOC.

[6] Here we present results of a unique set of multi-decadal global ocean model simulations employing both a strongly-eddying and a non-eddying configuration of the same ocean code. The models are forced with two types of freshwater flux perturbations; one spread over a broad band of the subpolar North Atlantic (as in traditional "hosing" experiments), while the other is distributed in a more realistic spatial and temporal pattern around the coast of Greenland. The latter distribution is inspired by studies of present-day runoff from the GrIS [*Rignot and Kanagaratnam*, 2006]. In these idealized experiments, a strong freshwater flux

[1]Los Alamos National Laboratory, Los Alamos, New Mexico, USA.
[2]New Mexico Consortium, Los Alamos, New Mexico, USA.
[3]Institute for Marine and Atmospheric Research, Utrecht, Netherlands.

Corresponding author: W. Weijer, Los Alamos National Laboratory, MS B216, Los Alamos, NM 87545, USA. (wilbert@lanl.gov)

0094-8276/12/2012GL051611

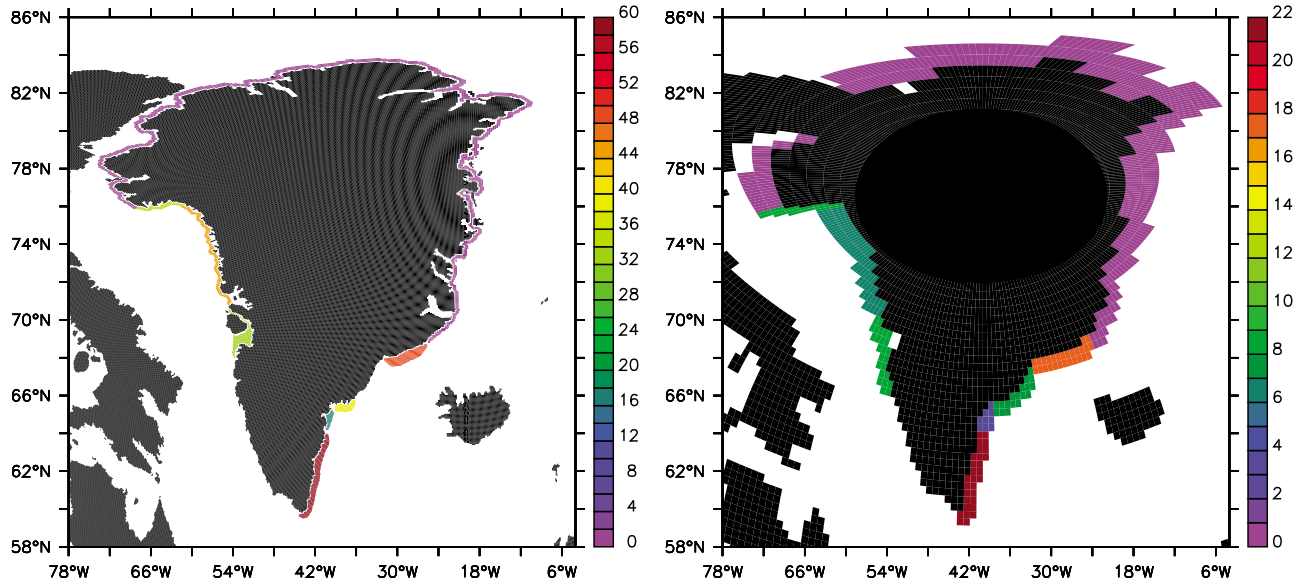

Figure 1. (left) Spatial distribution of the annual-mean Greenland freshwater discharge (in m/yr) for the strongly eddying configuration $R_{0.1}$, and (right) the low resolution configuration $x1$ for an integrated freshwater input of 0.1 Sv. The anomalous run off was applied with a seasonal cycle which peaks in July.

perturbation (0.1 Sv) is applied to emphasize differences in the response in the two configurations.

2. Experimental Approach

[7] To study the response of the AMOC we perform numerical experiments with global versions of Los Alamos' Parallel Ocean Program (POP). The higher-resolution version of the model has a nominal grid spacing of 0.1°, which allows the explicit representation of energetic mesoscale features including eddies and boundary currents [*Maltrud et al.*, 2008, 2010]. By using this strongly-eddying configuration of POP (referred to here as the $R_{0.1}$, or 'point-one'), this study is capable of providing the most accurate oceanographic depiction of AMOC response to enhanced freshwater flux due to GrIS melting to date. The lower-resolution, non-eddying version of the model ($x1$, or 'by-one') is presented on the same nominally 1° grid as used in version 3 of the Community Climate System Model, CCSM3 [*Collins et al.*, 2006], which makes use of explicit parameterizations to represent eddy-induced transports. The set up of the two models is as similar as practically possible, and the ocean states are in close agreement. The auxiliary material provides a more detailed description and validation of the models.[1]

[8] For both configurations a control (C-Mixed) and two perturbation simulations (E-Greenland and E-Hosing) were performed for at least 50 years each. The ocean models were forced by an annually repeating atmospheric climatology; these boundary conditions may overestimate the sensitivity of the AMOC to freshwater perturbations, as they ignore a stabilizing thermal feedback between the ocean and the atmosphere [*Rahmstorf*, 1995b; *Gerdes et al.*, 2006]. In addition, they do not include the warming that is thought to lead to the GrIS mass deficit in the first place, and which may lead to a slow-down of the AMOC by itself [*Mikolajewicz et al.*, 2007].

[9] The freshwater flux perturbation experiments are referred to as E-Hosing when the enhanced runoff is applied over a broad swath (50°N–70°N) of the northern North Atlantic, and as E-Greenland when distributed around the periphery of Greenland. The spatial distribution (Figure 1) is based on observed values of run-off and calving [*Rignot and Kanagaratnam*, 2006], and is characterized by high values of freshwater release on the southeastern and western flanks of Greenland, smaller values in the north and northeast, and no discharge for the southwest. Although it is unlikely that the spatial pattern of meltwater discharge will remain unaltered in a warming climate, a simple amplification of the current discharge distribution can be considered a best first guess.

[10] Observations suggest that the mass deficit has increased from almost zero to 267 ± 38 Gt/yr in 2007 [*Rignot et al.*, 2008]. This is equivalent to a freshwater flux increase of 0.009 ± 0.001 Sv (1 Sv = 10^6 m^{3}s^{-1}). Further increases in the mass deficit are expected in the coming decades, as both precipitation and surface melting are expected to increase in response to rising temperatures [*Mernild et al.*, 2010]. However, the largest uncertainty in freshwater flux projections is related to the dynamic response of the GrIS to higher air temperatures, and to higher ocean temperatures at the sites where outlet glaciers discharge into the ocean.

[11] Lacking reliable dynamic projections, we apply an integrated freshwater flux of 0.1 Sv in our simulations [*Stouffer et al.*, 2006; *Gerdes et al.*, 2006]. Being an order of magnitude larger than the flux implied by the current mass deficit of the GrIS, this rate can be considered a worst case scenario if the GrIS were to undergo a catastrophic collapse. To put this value in perspective, freshwater discharge by the Amazon river is of the order of 0.2 Sv [*Molinier et al.*, 1995], the armada of icebergs that entered the North Atlantic ocean during Heinrich Event 4 may have been equivalent to about 0.3 Sv [*Roche et al.*, 2004], while the Lake Agassiz

[1]Auxiliary materials are available in the HTML. doi:10.1029/2012GL051611.

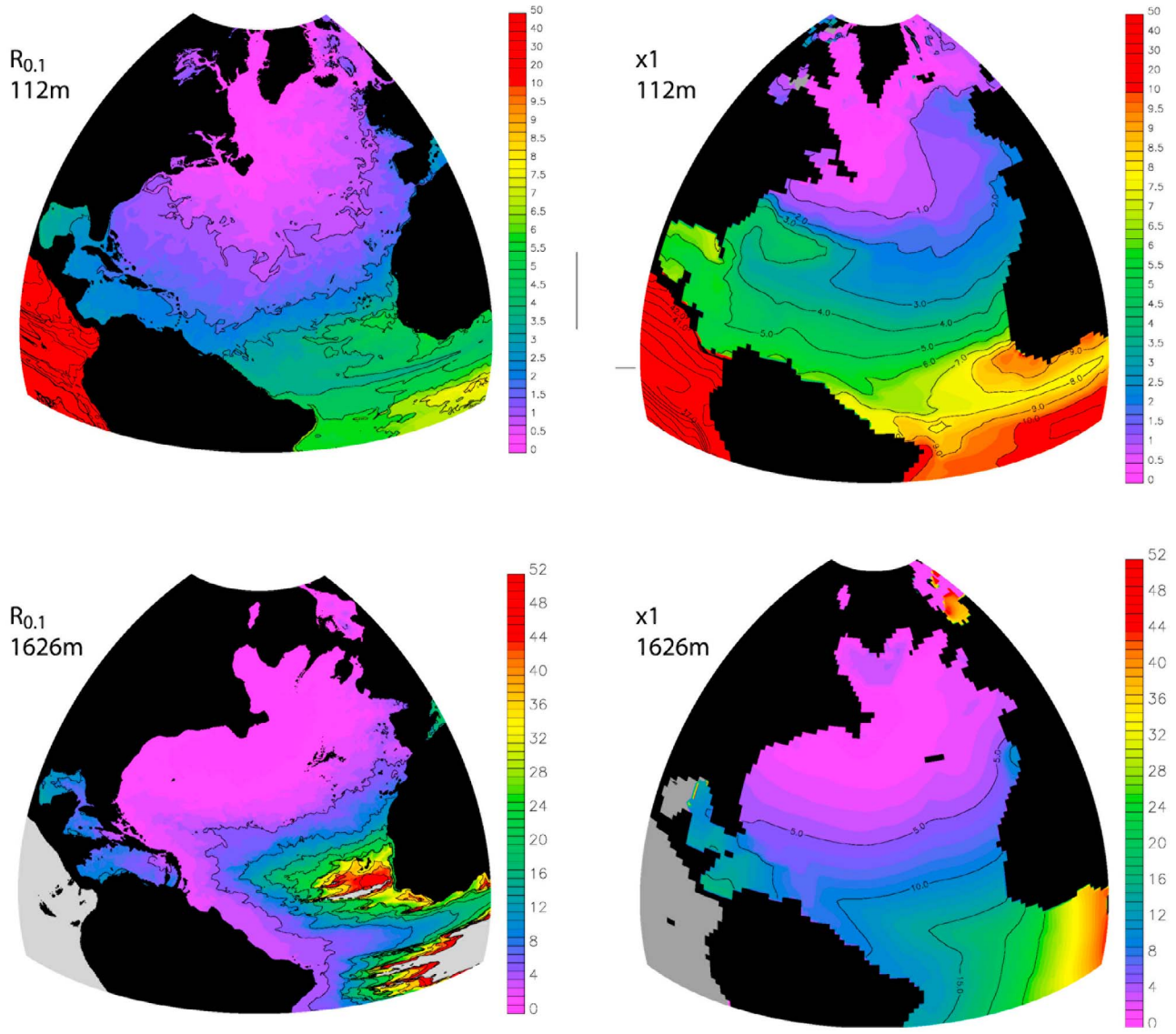

Figure 2. Arrival time (in years) for the dye in the (left) $R_{0.1}$ and (right) $x1$ configurations, at depths of (top) 112 m (contours at 1-year intervals) and (bottom) 1626 m (contours at 5-year intervals). Grey denotes arrival times greater than 50 years.

freshwater discharge (thought to have been responsible for the 8.2 kyr climate event) may have been equivalent to 0.17 Sv [*Hijma and Cohen*, 2010]. A substantial accumulation of fresh water in the Beaufort Gyre has recently been detected [*Giles et al.*, 2012], representing enough fresh water to produce a flux equivalent to 0.1 Sv over a period of nearly 3 years, when the wind forcing that contains it eventually shifts.

3. Results

[12] A major difference between the two models is the way tracers, including salinity, are transported through the ocean. To illustrate this difference, a passive dye was introduced along with the freshwater anomaly around Greenland. The arrival time of the dye was measured at each location to diagnose its dispersion rate. At shallow depths (Figure 2, top) a main area of discrepancy is the western subtropical gyre of the North Atlantic. In the strongly-eddying case ($R_{0.1}$) the more energetic circulation disperses the dye throughout the entire subtropical gyre in just 1 or 2 years. In contrast, in the non-eddying $x1$ the dispersion takes place mainly through advection by the mean gyre circulation. Consequently, it takes up to 5 years for the dye to reach the eastern seaboard of North America through this mean-advective route. Faster mean currents and eddies also deliver the dye more rapidly towards the south, with the dye reaching the equator in less than 5 years in the $R_{0.1}$, while it takes about 8 years in the $x1$.

[13] At depth (Figure 2, bottom) the differences are even more striking; in the $R_{0.1}$ it takes less than 5 years for the dye to reach the deep western boundary current off Brazil, while in the $x1$ this takes between 10 and 15 years. In the eastern Atlantic off Africa, between 5° and 20° from the equator, the $R_{0.1}$ displays shadow zones where even after 50 years no dye has penetrated. No such isolated pools are present in the $x1$ results (although it takes almost 4 decades for the signal to reach the Guinea and Angola Basins).

[14] The freshwater input and associated surface freshening has a strong impact on the deep water formation process

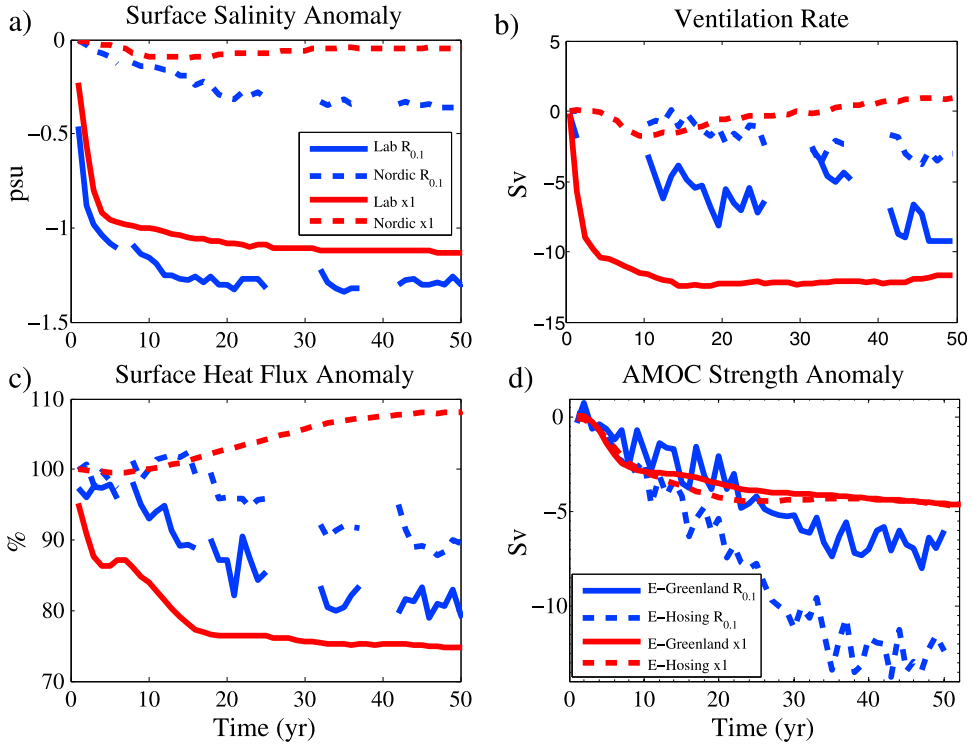

Figure 3. Responses of the $R_{0.1}$ (blue) and $x1$ (red) configurations to a 0.1 Sv integrated input of freshwater. (a) Anomalous (E-Greenland minus C-Mixed) area-averaged annual sea surface salinity in the Labrador (solid) and Nordic (dashed) seas. (b) Anomalous rate of ventilation, defined as the area-integrated maximum mixed-layer depth in March, divided by the number of seconds per year [*Gerdes et al.*, 2005]. (c) Relative anomaly of area-averaged annual surface heat flux. (d) Anomalous maximum overturning strength for the E-Greenland (solid) and E-Hosing (dashed) experiments. In the E-Greenland experiments the freshwater flux perturbation is applied in a narrow strip around Greenland, while in E-Hosing it is applied homogeneously over a broad swath (50°N–70°N) in the northern North Atlantic. Absolute values of maximum AMOC are shown in Figure S1 in Text S1. Time (in years) is relative to the branch-off point at year 75. Gaps in the results of the $R_{0.1}$ configuration are due to data loss, as explained in the Computational Considerations section of the auxiliary material.

in the Labrador and Nordic Seas. The strongest discharges from the GrIS are within, and upstream of the Labrador Sea, and here sea surface salinities (SSS) are impacted most strongly (Figure 3a); mean SSS in the Labrador Sea shows a dramatic drop of about 1 psu in the first few years of the perturbation experiments. The temporal evolution of the salinity field at the surface, and at depth (Figure S3 in Text S1), are remarkably similar in the two models. Nonetheless, there is marked difference in the response of deep convection in this basin. In the $x1$ the drop in SSS is accompanied by a dramatic decrease in the rate of ventilation (Figure 3b): a 10 Sv decline in the first 3 years (equivalent to 30% compared to the C-Mixed control integration) is followed by an additional 2 Sv decrease in the subsequent decade. This reduction in ventilation is associated with a 25% reduction in ocean surface heat loss (Figure 3c). In the $R_{0.1}$ case the decline in convective activity is much more gradual, as the convective volume slowly declines to a 10 Sv (40%) deficit after 50 years, accompanied by a gradual decrease in surface heat loss to 80% of the C-Mixed value. We speculate that this difference in the response of deep convection in the Labrador Sea must be attributed to the high spatial variance of SSS in the $R_{0.1}$, as the explicit resolution of meso-scale features leads to strong filamentation of the buoyancy field.

[15] The situation in the Nordic Seas is more complicated. With the freshwater discharges on the eastern and northern sides of Greenland being much weaker than those influencing the Labrador Sea, the decline in SSS is less dramatic here. This is also reflected in the changes in convective activity: the net reduction in ventilation rate in the $R_{0.1}$ is just 3 Sv (15%) over 50 years, associated with a 10% reduction in net surface heat loss. In contrast, in the $x1$ the rate of ventilation increases by 1 Sv (4%), associated with an 8% increase in net surface heat loss. This counterintuitive response is due to a combination of factors. First, there is a distinct difference in the background salinity distribution of the Nordic Seas between the two models. In particular, the $x1$ shows a clear salinity maximum at a depth of about 300 m (Figure S3 in Text S1), a feature that is absent in the $R_{0.1}$, and only weakly present in observations. Second, in both models the Greenland freshwater discharge leads to a strengthening of the cyclonic circulation in the Nordic Seas and an associated doming of the isopycnals. This doming brings the high-salinity layer of the $x1$ closer to the surface, reducing the static stability of the water column, and facilitating deep convection and enhanced surface heat loss. This mechanism is different from the one put forward by *Kleinen et al.* [2009]: they observed a strong subsurface warming in the Nordic Seas in response to anomalous freshwater input, resulting from an enhanced heat import from the

subpolar North Atlantic; a similar warming is clearly absent here.

[16] The overall decline in convective activity is reflected by a weakening of the AMOC in both models (Figure 3d). In the $x1$, the dramatic reduction in ventilation rate in the Labrador Sea leads to an abrupt decrease in AMOC strength of about 3 Sv in the first 8 years, followed by a more gradual adjustment on decadal time scales as the convective activity reaches a new equilibrium. This behavior is very similar to that found before in models of comparable resolution [*Stammer*, 2008]. In contrast, the adjustment in the high-resolution model is fundamentally gradual and more persistent, consistent with the gradual decline in ventilation rates in both the Labrador and Nordic Seas. Only after 35 years does the decline in overturning strength show signs of leveling off.

[17] In fact, the ultimate reduction in AMOC strength in the $R_{0.1}$ is greater than in the $x1$ case; the cross-over takes place after about 20 years. A conclusive explanation for this difference is still lacking; we found that a simple relationship between AMOC strength and meridional pressure difference, as found in some coarse-resolution ocean models [*Griesel and Morales Maqueda*, 2006], does not hold in the models considered here. We hypothesize that the increase in Nordic Seas ventilation in the $x1$ mitigates the reduced convection in the Labrador Sea, reducing the long-term impact of the freshwater flux anomaly on the strength of the AMOC.

[18] The mechanistic view of AMOC response described above is supported by the results of the E-Hosing simulations (Figure 3d, dashed curves). In the $x1$ the response hardly differs between the E-Greenland and E-Hosing cases, as SSS over the convective sites and the ventilation rates are only modestly different (Figure S4 in Text S1). This suggests that the AMOC in low-resolution models is quite insensitive to the manner in which the freshwater flux is applied, consistent with previous studies [*Kleinen et al.*, 2009]. In contrast, in the $R_{0.1}$ the response is much stronger when the freshwater is imposed broadly through hosing than when applied within the coastal waters off of Greenland. In the E-Greenland experiment, strong and narrow boundary currents efficiently remove the coastally-trapped freshwater anomalies from the subpolar basins, preventing them from optimally affecting the convective sites in the basin interiors (Figure S4 in Text S1).

4. Summary and Conclusions

[19] In this paper we present results of the first-ever multi-decadal sensitivity study of the AMOC in a global, strongly-eddying ocean model. We study the impact of enhanced melt water input from the GrIS on the AMOC and convection in the subpolar North Atlantic, and compare the response to that in an identically configured, non-eddying IPCC-class ocean model. Our results show that the decadal response of the AMOC to enhanced melt water input is quantitatively similar (to within 10%) in the two models. Nonetheless, significant differences were found in the transient response of the AMOC and wintertime convection in the Labrador Sea. In the non-eddying model ventilation rates are reduced abruptly (10 Sv in the first 3 years), a response mirrored by a rapid decline of the AMOC (3 Sv in the first 8 years). In the strongly-eddying model the adjustments are more gradual; both the wintertime convection and the AMOC take many decades to adjust.

[20] The results furthermore show that for the non-eddying model the response of the AMOC is not sensitive to the spatial pattern of the freshwater flux perturbation. This indicates that the many lower-resolution hosing experiments performed to date may have produced very similar results if the freshwater flux had been applied more realistically to the coastal waters around Greenland. The difference is much more pronounced in the strongly-eddying case, where the rapid reduction of the AMOC in response to a hosing freshwater flux contrasts with the more gradual response in the E-Greenland case.

[21] Given the limitations of the experimental set-up, it can be assumed that the strongly-eddying model displays the most accurate response, as i) its ocean state is closer to observations than the non-eddying model, ii) its dynamics are more strongly controlled by fundamental fluid dynamics and are less reliant on parameterizations, and iii) the bathymetry is better resolved. Nonetheless, more comparative studies are necessary to test the robustness of these results, especially when including an active atmosphere, in order to gain a full appreciation of the climate responses in these dynamically rich models, which will become the standard for ocean climate models in the near future.

[22] **Acknowledgments.** This research was supported by the Climate Change Prediction Program of the U.S. Department of Energy Office of Science. Los Alamos National Laboratory is operated by the Los Alamos Natio Security, LLC for the National Nuclear Security Administration of the U.S. Department of Energy under contract DE-AC52-06NA25396. The computations were done on the Huygens IBM Power6 at SARA in Amsterdam, the Institutional Computing facilities at Los Alamos National Laboratory, and the Jaguar supercomputer at the National Center for Computational Sciences at Oak Ridge National Laboratory. Use of the SARA computing facilities was sponsored by the National Computing Facilities Foundation (N.C.F.) under the project SH084-08 with financial support from the Netherlands Organization for Scientific Research (NWO). The authors would like to thank S. Mernild, S. Price and N. Jeffery (LANL), M. den Toom (IMAU), and F. Primeau (UC Irvine) for useful discussions, and two anonymous reviewers for constructive comments.

[23] The Editor thanks two reviewers for assisting with the evaluation of this paper.

References

Bower, A., M. Lozier, S. Gary, and C. Böning (2009), Interior pathways of the North Atlantic meridional overturning circulation, *Nature*, *459*(7244), 243–247.

Brambilla, E., and L. D. Talley (2006), Surface drifter exchange between the North Atlantic subtropical and subpolar gyres, *J. Geophys. Res.*, *111*, C07026, doi:10.1029/2005JC003146.

Broecker, W. S. (1991), The great ocean conveyor, *Oceanography*, *4*(2), 79–89.

Collins, W. D., et al. (2006), The Community Climate System Model Version 3 (CCSM3), *J. Clim.*, *19*, 2122–2143.

Cunningham, S., et al. (2007), Temporal variability of the Atlantic meridional overturning circulation at 26.5° N, *Science*, *317*(5840), 935.

Drijfhout, S., E. Maier-Reimer, and U. Mikolajewicz (1996), Tracing the conveyor belt in the Hamburg large-scale geostrophic ocean general circulation model, *J. Geophys. Res.*, *101*(22), 22,563–22,576.

Gerdes, R., J. Hurka, M. Karcher, F. Kauker, and C. Koberle (2005), Simulated history of convection in the Greenland and Labrador Seas, 1948–2001, in *The Nordic Seas: An Integrated Perspective*, *Geophys. Monogr. Ser.*, vol. 158, pp. 221–238, AGU, Washington, D. C.

Gerdes, R., W. Hurlin, and S. M. Griffies (2006), Sensitivity of a global ocean model to increased run-off from Greenland, *Ocean Modell.*, *12*(3–4), 416–435.

Giles, K. A., S. W. Laxon, A. L. Ridout, D. J. Wingham, and S. Bacon (2012), Western Arctic Ocean freshwater storage increased by wind-driven spin-up of the Beaufort Gyre, *Nat. Geosci.*, doi:10.1038/ngeo1379, in press.

Griesel, A., and M. A. Morales Maqueda (2006), The relation of meridional pressure gradients to North Atlantic Deep Water volume transport in an ocean general circulation model, *Clim. Dyn.*, *26*, 781–799.

Hijma, M. P., and K. M. Cohen (2010), Timing and magnitude of the sea-level jump preluding the 8200 yr event, *Geology*, *38*(3), 275–278, doi:10.1130/G30439.1.

Kleinen, T., T. J. Osborn, and K. R. Briffa (2009), Sensitivity of climate response to variations in freshwater hosing location, *Ocean Dyn.*, *59*, 509–521.

Lozier, M. S. (2010), Deconstructing the Conveyor Belt, *Science*, *328*(5985), 1507–1511.

Maier-Reimer, E., and U. Mikolajewicz (1989), Experiments with an OGCM on the cause of the Younger Dryas, *Rep. 39*, Max-Planck-Inst. für Meteorol., Hamburg, Germany.

Maltrud, M., F. Bryan, and S. Peacock (2010), Boundary impulse response functions in a century-long eddying global ocean simulation, *Environ. Fluid Mech.*, *10*(1), 275–295.

Maltrud, M. E., F. Bryan, M. Hecht, E. Hunke, D. Ivanova, J. McClean, and S. Peacock (2008), Global ocean modelling in the eddying regime using POP, *CLIVAR Exchanges*, *44*, 5–8.

Marsh, R., D. Desbruyères, J. L. Bamber, B. A. de Cuevas, A. C. Coward, and Y. Aksenov (2010), Short-term impacts of enhanced Greenland freshwater fluxes in an eddy-permitting ocean model, *Ocean Sci.*, *6*, 749–760.

Mernild, S. H., G. E. Liston, C. A. Hiemstra, and J. H. Christensen (2010), Greenland ice sheet surface mass-balance modeling in a 131-yr perspective, 1950–2080, *J. Hydrometeorol.*, *11*(1), 3–25, doi:10.1175/2009JHM1140.1.

Mikolajewicz, U., M. Vizcaíno, J. Jungclaus, and G. Schurgers (2007), Effect of ice sheet interactions in anthropogenic climate change simulations, *Geophys. Res. Lett.*, *34*, L18706, doi:10.1029/2007GL031173.

Molinier, M., J. L. Guyot, E. De Oliveira, V. Guimarães, and A. Chaves (1995), Hydrologie du bassin de l'Amazone, *Proc. Grands Bassins Fluviaux Periatlantiques*, *1*, 335–344.

Rahmstorf, S. (1995a), Bifurcations of the Atlantic thermohaline circulation in response to changes in the hydrological cycle, *Nature*, *378*, 145–149.

Rahmstorf, S. (1995b), Multiple convection patterns and thermohaline flow in an idealized OGCM, *J.Clim.*, *8*, 3028–3039.

Rignot, E., and P. Kanagaratnam (2006), Changes in the velocity structure of the Greenland Ice Sheet, *Science*, *311*(5763), 986–990, doi:10.1126/science.1121381.

Rignot, E., J. Bamber, M. Van den Broeke, C. Davis, Y. Li, W. Van de Berg, and E. Van Meijgaard (2008), Recent Antarctic ice mass loss from radar interferometry and regional climate modelling, *Nat. Geosci.*, *1*(2), 106–110.

Roche, D., D. Paillard, and E. Cortijo (2004), Constraints on the duration and freshwater release of Heinrich event 4 through isotope modelling, *Nature*, *432*(7015), 379–382.

Rooth, C. (1982), Hydrology and ocean circulation, *Prog. Oceanogr.*, *11*, 131–149.

Stammer, D. (2008), Response of the global ocean to Greenland and Antarctic ice melting, *J. Geophys. Res.*, *113*, C06022, doi:10.1029/2006JC004079.

Stommel, H. (1961), Thermohaline convection with two stable regimes of flow, *Tellus*, *2*, 224–230.

Stouffer, R. J., et al. (2006), Investigating the causes of the response of the thermohaline circulation to past and future climate changes, *J. Clim.*, *19*, 1365–1387.

van den Broeke, M., J. Bamber, J. Ettema, E. Rignot, E. Schrama, W. J. van de Berg, E. van Meijgaard, I. Velicogna, and B. Wouters (2009), Partitioning recent Greenland mass loss, *Science*, *326*(5955), 984–986, doi:10.1126/science.1178176.

Velicogna, I. (2009), Increasing rates of ice mass loss from the Greenland and Antarctic ice sheets revealed by GRACE, *Geophys. Res. Lett.*, *36*, L19503, doi:10.1029/2009GL040222.

Wu, X., M. B. Heflin, H. Schotman, B. L. A. Vermeersen, D. Dong, R. S. Gross, E. R. Ivins, A. W. Moore, and S. E. Owen (2010), Simultaneous estimation of global present-day water transport and glacial isostatic adjustment, *Nat. Geosci.*, *3*, 642–646.

Supplementary Information to: Response of the Atlantic Ocean Circulation to Greenland Ice Sheet Melting in a Strongly-Eddying Ocean Model

Strongly-eddying configuration: $R_{0.1}$

The fully global simulations described here were performed using the Parallel Ocean Program (POP [*Dukowicz and Smith*, 1994]) developed at Los Alamos National Laboratory. The strongly eddying configuration, indicated by $R_{0.1}$, is identical to that used by *Maltrud et al.* [2010], and features several refinements with respect to the set-up used by Maltrud and McClean (2005) [*Maltrud and McClean*, 2005]. The horizontal grid has a nominal longitudinal resolution of 0.1°, and has a tripole layout [*Murray*, 1996] with poles in Canada and Russia. There are 42 vertical levels, allowing for a maximum depth of 6000 m. Bottom topography is discretized as partial bottom cells [*Adcroft et al.*, 1997], creating a more accurate and smoother representation of topographic slopes than the traditional full-cell approach.

Biharmonic formulations are used for horizontal viscosity (ν_0) and diffusivity of tracers (κ_0), both with a cubic dependence on local grid size [*Maltrud et al.*, 1998]. Explicit dissipation is weak, with equatorial values of $\nu_0 = -90\ \mathrm{m^4 s^{-1}}$ for momentum and $\kappa_0 = -30$

m^4s^{-1} for tracers. Vertical mixing coefficients for momentum and tracers are calculated by an implementation of the K-Profile Parameterization [*Large et al.*, 1994] that includes the use of large diffusion coefficients (0.1 m^2s^{-1}) to resolve gravitational instabilities. Background values for vertical tracer diffusion range from 10^{-5} m^2s^{-1} near the surface to 10^{-4} m^2s^{-1} at depth, with viscosity values an order of magnitude higher. A highly accurate and efficient equation of state is used to calculate density of sea water [*McDougall et al.*, 2003]. Initial temperature and salinity fields were interpolated from the annual mean WOCE Global Hydrographic Climatology [*Gouretski and Koltermann*, 2004].

Non-eddying configuration: $x1$

In order to make a meaningful evaluation of the AMOC response, the low-resolution model was configured to be consistent with the high-resolution model, where possible. The model, indicated by $x1$, has the nominal 1° horizontal resolution of the Community Climate System Model. The layout of the grid is dipolar, with the northern pole displaced onto Greenland; the vertical grid consists of 40 levels, reaching a maximum depth of 5500 m (vertical grid spacing are identical to those of the higher resolution model). As in the CCSM, the partial bottom cell approach is not applied. Tracer diffusion is accomplished by the Gent & McWilliams eddy transport scheme [*Gent and McWilliams*, 1990], while an anisotropic Laplacian formulation is used for viscosity [*Smith and McWilliams*, 2003].

Surface forcing

Since this study focuses on the impact of explicitly resolved mesoscale transports on the decadal response of the AMOC to freshwater flux perturbations, we chose to restrict the timescales introduced by the surface forcing. The atmospheric state was based on the

repeat annual cycle (normal-year) Coordinated Ocean Reference Experiment (CORE) forcing dataset [*Large and Yeager*, 2004], with the 6-hourly forcing averaged to monthly. This choice leaves the seasonal cycle as the only externally enforced time scale in the system; all variability on interannual and intraseasonal time scales is therefore internally generated. Wind stress was calculated offline using the Hurrell Sea Surface Temperature (SST) climatology [*Hurrell et al.*, 2008] and standard bulk formulae [*Large and Pond*, 1982]. Evaporation and sensible heat flux were calculated online also using bulk formulae and the model predicted SST. Precipitation was also taken from the CORE forcing dataset. Monthly river runoff from 46 major rivers [*Fekete et al.*, 2000] was added to the freshwater flux at the locations of the actual outflow, with the remaining ungauged runoff distributed evenly along the coasts of all of the continents. This distribution also accounts for the climatological run-off from Greenland. Ice cover was prescribed based on the -1.8°C isoline of the SST climatology, with both temperature and salinity restored on a timescale of 30 days under diagnosed climatological ice.

In both configurations, 75-year spin-up simulations were performed (starting from rest) with this prescribed annually repeating atmospheric state, using weak restoring of surface salinity to global climatology to control salinity drift (referred to as C-Restore). However, this approach is inconsistent with a freshwater flux perturbation experiment, since such a forcing tends to artificially remove the perturbation [*Marsh et al.*, 2010]. To avoid this problem, the restoring flux was diagnosed during years 76-80 of the spin-up runs, and the monthly-averaged flux from this 5 year period was then used in a "mixed boundary condition" formulation to control drift (instead of restoring) in the control and perturba-

tion simulations to be described here. Upon switching to mixed boundary conditions, the AMOCs in the control runs (referred to as C-Mixed) do not show signs of collapse as in previous studies [*Griffies et al.*, 2009]. Instead, the overturning circulations remain strong and stable and display only a slight adjustment ($< 10\%$) compared to the C-Restore spin-up runs (Fig. S1), suggesting that the switch of boundary conditions maintains a well-balanced overturning state.

The freshwater perturbation experiments (the E cases) are subjected to a similar switch in boundary conditions as the C-Mixed experiments, in addition to the application of the flux anomalies. To evaluate the AMOC response to these flux anomalies, we present the changes with respect to the C-Mixed runs, necessarily assuming that the responses to the switch in boundary conditions and to the applied flux are independent.

All freshwater fluxes are converted to virtual fluxes of salinity in order to assure volume conservation. Application of the same virtual salinity flux in both configurations generates similar density perturbations, allowing for a fair comparison of the ocean response. However, this approach neglects the fact that the input of a certain amount of freshwater has less impact on the salinity of a fresher water parcel than on the salinity of a saltier parcel [*Griffies et al.*, 2005]. With the Labrador and Nordic Seas being slightly fresher in the $R_{0.1}$ configuration (e.g., Fig. S3), the actual response might be slightly overestimated.

Evaluation

The representation of the ocean state in the two configurations is very similar, and in general compares well with observations: the maximum value of the overturning streamfunction in the Atlantic (the strength of the AMOC) is 23.9 Sv in the $R_{0.1}$ and 23.6 Sv

in the $x1$ when averaged over the first 5 years of the C-Mixed experiment, and 25.4 Sv vs. 24.1 Sv when averaged over the entire 50 years (Figs. S1 and S2). The overturning strengths of 21 Sv ($R_{0.1}$) and 20 Sv ($x1$) at latitude 26.5°N compare well with the 18.7 ± 5.6 Sv observational estimate from the RAPID array [*Cunningham et al.*, 2007].

Still, the ocean states represented by the C-Mixed cases display some differences: i) the 50-year averages of mean sea surface salinity in the Labrador and Nordic Seas are slightly higher in the $x1$ configuration (33.98 and 34.81 psu, respectively) than in the $R_{0.1}$ (33.67 and 34.63 psu) and observations [*Antonov et al.*, 2010] (33.15 and 34.34 psu); ii) subsurface salinity profiles in the Labrador and Nordic Seas are closer to climatology in the $R_{0.1}$ configuration (Fig. S3). Still, a subsurface salinity maximum in the observations is absent in the strongly-eddying model, while it is exaggerated in the non-eddying configuration; iii) rates of deep ventilation (estimated by the area-integrated March mixed layer depth, where deeper than 1500 m, divided by the number of seconds per year) is on average 14.3 Sv in the Labrador Sea and 0.5 Sv in the Nordic Seas in the $R_{0.1}$. These values are typical of strong positive phases of the North Atlantic Oscillation [*Gerdes et al.*, 2005]. No convection deeper than 1500 m takes place in the Nordic or Labrador Seas in the $x1$. *Total* ventilation rates (the area-integrated March mixed layer depth, divided by the number of seconds per year) are stronger in the $x1$, with rates of 30.8 Sv and 23.3 Sv in the Labrador and Nordic Seas, respectively, vs. 24.4 and 16.9 Sv in the $R_{0.1}$; iv) Annually averaged surface heat fluxes in the Labrador and Nordic Seas are high compared to reanalyses. The $R_{0.1}$ configuration has mean surface heat losses of 88.4 and 75.6 W m^{-2} in the Labrador and Nordic Seas respectively, compared to 63.2 and 82.9 W m^{-2}

for the $x1$, with only weak interannual variability. The comparable metric in the NCEP reanalysis indicates values of only 26.4 $\pm$ 10.4 and 48.2 $\pm$ 9.4 W m^{-2} for the 1948-2005 period [*Kalnay et al.*, 1996], although this variable is poorly constrained by observations.

E-Hosing response

The main differences between the E-Hosing and E-Greenland experiments are illustrated in Fig. 4. The SSS in the climatological convection sites in the Labrador and Nordic Seas do not change much in the $x1$ model: the Labrador Sea is a bit saltier in the E-Hosing experiment, while the Nordic Seas are bit fresher, as can be expected when the freshwater input is changed from a concentrated discharge around Greenland to a homogeneous distribution over the 50°-70°N band. The situation is different in the $R_{0.1}$ case, where the convection sites in both the Nordic and Labrador Seas become increasingly fresher in the E-Hosing experiment. It is obvious that in the E-Greenland case the freshwater has trouble reaching the deep convection sites in both basins. The main reason for this is that the strong boundary current flushes out the coastally-trapped freshwater anomalies before they can optimally affect the convection sites in the basin interiors. The broader band of freshwater discharge, the broader and more sluggish currents, and the stronger horizontal diffusion in the $x1$ configuration are likely factors that allow the freshwater anomalies to reach the convective sites more efficiently.

These differences in surface salinity response are also reflected in the ventilation rates Fig. 4b. In the $x1$, ventilation rates in the Nordic Seas are hardly different for the two scenarios, while Labrador Sea convection remains stronger in the E-Hosing case compared to E-Greenland, consistent with the saltier surface waters. This is largely offset by a

decrease in convective activity in the subpolar North Atlantic (not shown). In contrast, in the $R_{0.1}$ convection in both basins is reduced in the E-Hosing, compared to E-Greenland. This is consistent with the increasing freshening of the convective sites in the E-Hosing case, and explains the stronger reduction in AMOC strength, compared to E-Greenland.

Computational considerations

Each of the multi-decadal runs of the strongly-eddying model cost in excess of 1M cpu hrs on the high-performance platforms available to us. These requirements obviously limit the number of simulations that can be performed. The current results depend on a single realization per experiment, which prevents a proper statistical analysis of their significance. Monthly output of the most relevant model fields requires on the order of 10 Gb in storage space, limiting the number of 3-dimensional model fields that can be saved.

For some of the $R_{0.1}$ runs we experienced some data loss. The temporary storage system where the output is written out applies an agressive scrubbing policy that removes files that have not been touched for a couple of weeks; failure to move the files to archival storage in time has resulted in some loss of data.

References

Adcroft, A., C. Hill, and J. Marshall (1997), Representation of topography by shaved cells in a height coordinate ocean model, *Monthly Weather Review*, *125*(9), 2293–2315.

Antonov, J. I., D. Seidov, T. P. Boyer, R. A. Locarnini, A. V. Mishonov, H. E. Garcia, O. K. Baranova, M. M. Zweng, and D. R. Johnson (2010), World ocean atlas 2009, volume 2: Salinity, *NOAA Atlas NESDIS*, *69*, 184 pp.

Cunningham, S., et al. (2007), Temporal Variability of the Atlantic Meridional Overturning Circulation at 26.5° N, *Science*, *317*(5840), 935.

Dukowicz, J. K., and R. D. Smith (1994), Implicit free-surface method for the Bryan-Cox-Semtner ocean model, *J. Geophys. Res.*, *99*, 7991–8014.

Fekete, B. M., C. J. Vörösmarty, and W. Grabs (2000), Global, composite runoff fields based on observed river and simulated water balances, *Technical Report, Global Runoff Data Centre*.

Gent, P. R., and J. C. McWilliams (1990), Isopycnal mixing in ocean circulation models, *J. Phys. Oceanogr.*, *20*, 150–155.

Gerdes, R., J. Hurka, M. Karcher, F. Kauker, and C. Koberle (2005), Simulated history of convection in the greenland and labrador seas, 1948-2001, in *The Nordic seas: an integrated perspective*, *Geophysical monograph- American Geophysical Union*, vol. 158, pp. 221–238, American Geophysical Union.

Gouretski, V., and K. Koltermann (2004), WOCE global hydrographic climatology, *Berichte des BSH*, *35*, 1–52.

Griffies, S. M., et al. (2005), Formulation of an ocean model for global climate simulations, *Ocean Science*, *1*, 45–79.

Griffies, S. M., et al. (2009), Coordinated ocean-ice reference experiments (COREs), *Ocean Modelling*, *26*(1-2), 1–46.

Hurrell, J. W., J. J. Hack, D. Shea, J. M. Caron, and J. Rosinski (2008), A new sea surface temperature and sea ice boundary dataset for the community atmosphere model, *J. Clim.*, *21*(19), 5145–5153.

Kalnay, E., et al. (1996), The NCEP/NCAR 40-Year Reanalysis Project, *Bull. Amer. Meteorol. Soc.*, *77*, 437–471.

Large, W., and S. Pond (1982), Sensible and latent heat flux measurements over the ocean, *J. Phys. Oceanogr.*, *12*(5), 464–482.

Large, W. G., and S. Yeager (2004), Diurnal to decadal global forcing for ocean and sea-ice models: the data sets and flux climatologies, *Tech. rep.*, National Center for Atmospheric Research, Boulder, CO, U.S.A.

Large, W. G., J. C. McWilliams, and S. C. Doney (1994), Oceanic vertical mixing: A review and a model with nonlocal boundary layer parameters, *Rev. Geophys.*, *32*, 363–403.

Maltrud, M., F. Bryan, and S. Peacock (2010), Boundary impulse response functions in a century-long eddying global ocean simulation, *Environmental fluid mechanics*, *10*(1), 275–295.

Maltrud, M. E., and J. L. McClean (2005), An eddy-resolving global 1/10° ocean simulation, *Ocean Model.*, *8*, 31–54.

Maltrud, M. E., R. D. Smith, A. J. Semtner, and R. C. Malone (1998), Gobal eddy-resolving ocean simulations driven by 1985–1995 atmospheric winds, *J. Geophys. Res.*, *103*, 30,825–30,853.

Marsh, R., D. Desbruyères, J. L. Bamber, B. A. de Cuevas, A. C. Coward, and Y. Aksenov (2010), Short-term impacts of enhanced Greenland freshwater fluxes in an eddy-permitting ocean model, *Ocean Sci.*, *6*, 749–760.

McDougall, T., D. Jackett, D. Wright, and R. Feistel (2003), Accurate and computationally efficient algorithms for potential temperature and density of seawater, *J. Atmos. Ocean. Tech.*, *20*(5), 730–741.

Murray, R. (1996), Explicit generation of orthogonal grids for ocean models, *J. Comput. Phys.*, *126*(2), 251–273.

Smith, R. D., and J. C. McWilliams (2003), Anisotropic horizontal viscosity for ocean models, *Ocean Model.*, *5*, 129–156.

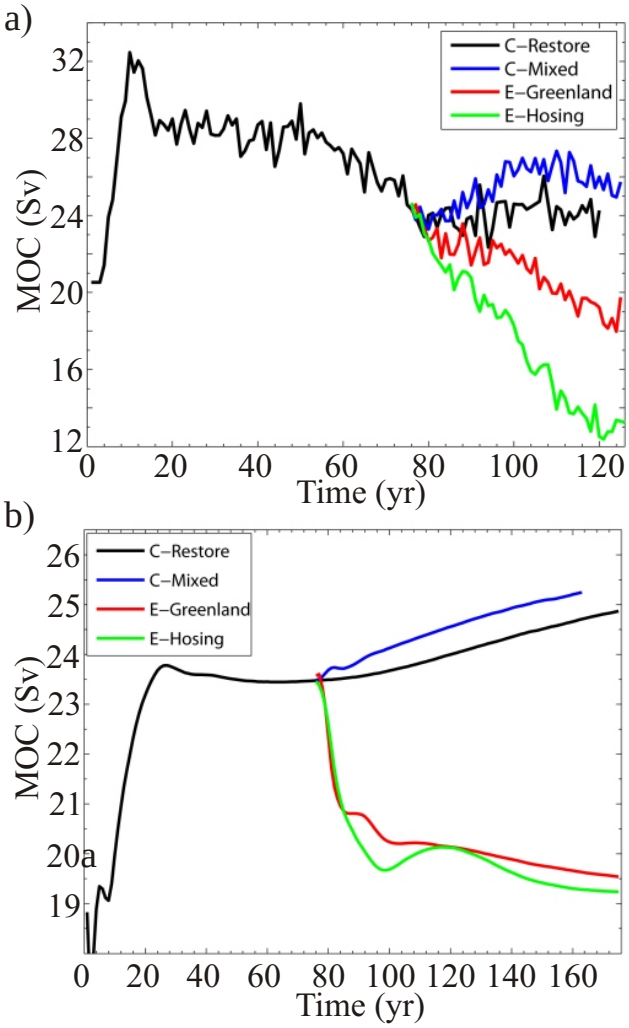

Figure S1. Maximum overturning strength in the Atlantic for the different integrations for a) the strongly eddying configuration $R_{0.1}$, and b) the low resolution configuration $x1$. Curves are for the control integrations with salinity relaxation (C-Restore; black), the control integations with mixed boundary conditions (C-Mixed; blue), the Greenland freshwater perturbation experiments (E-Greenland; red), and the traditional hosing experiments (E-Hosing; green).

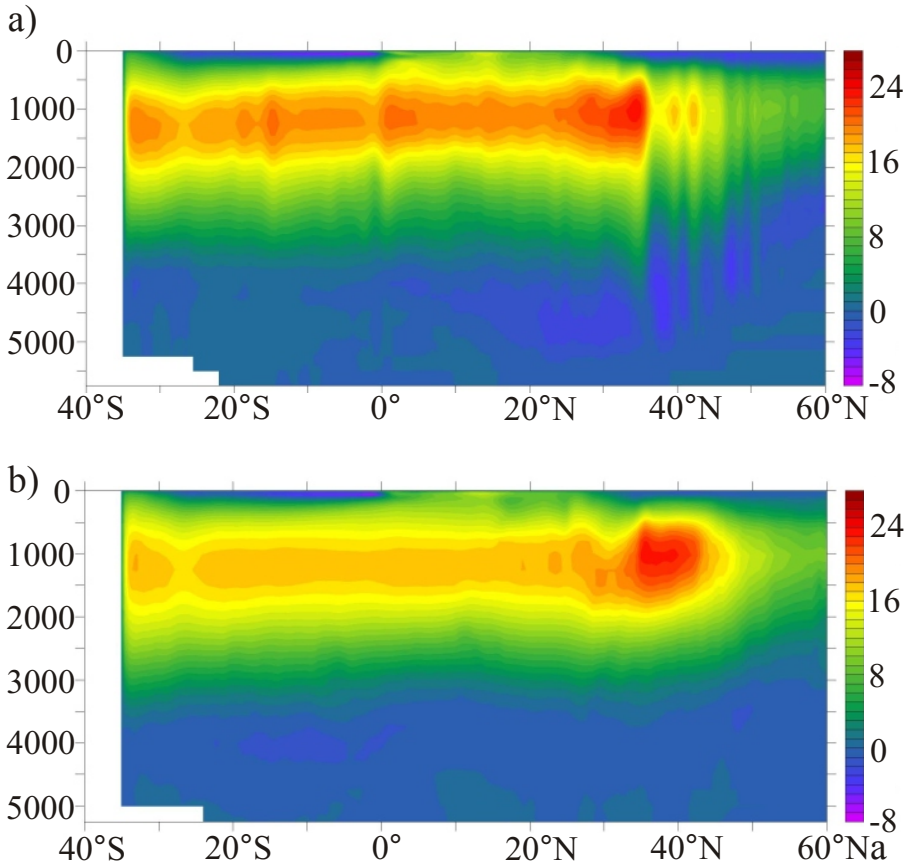

Figure S2. Atlantic Meridional Overturning streamfunction for the a) $R_{0.1}$ and b) $x1$ cases, averaged over years 1–10 of the C-Mixed integrations.

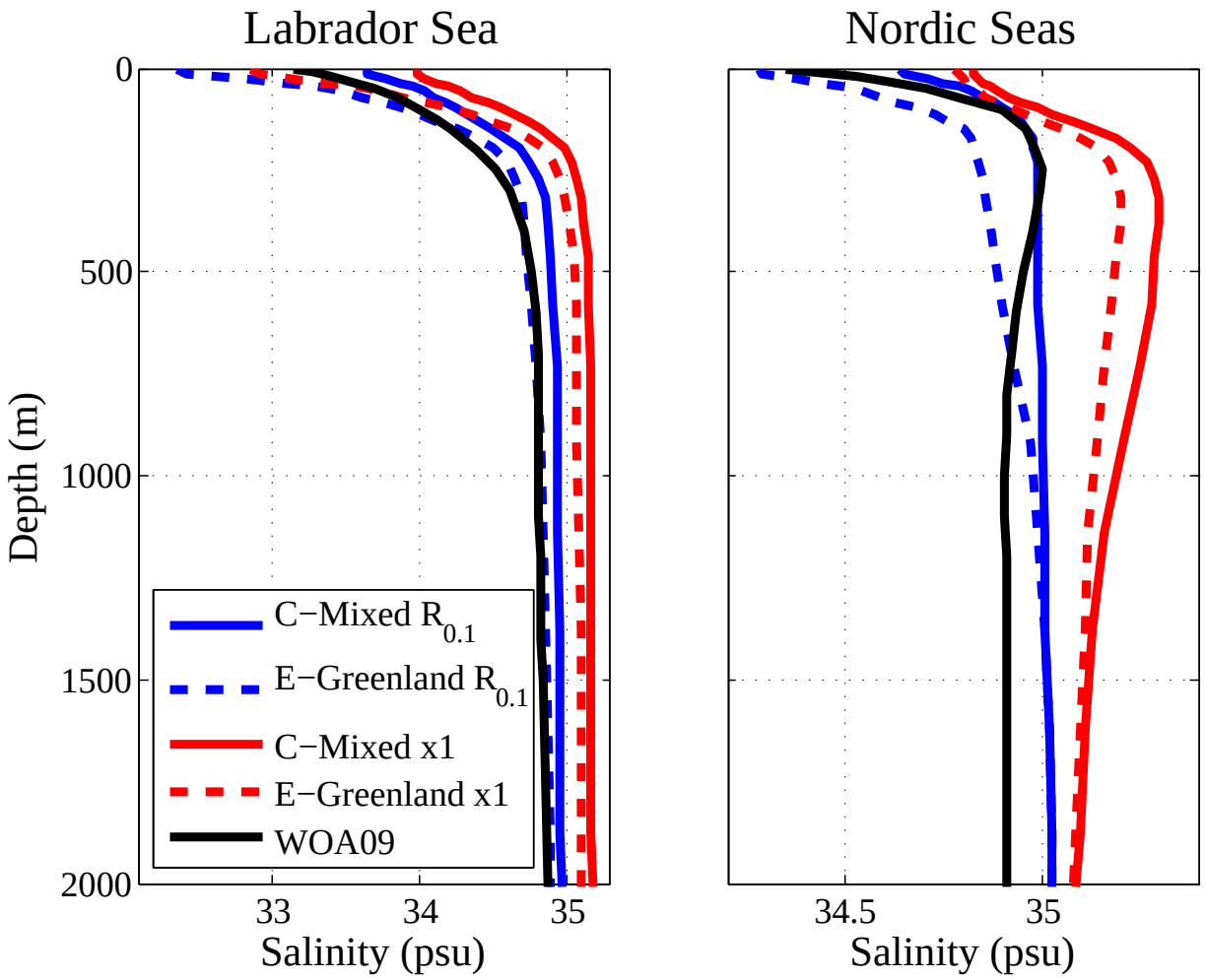

Figure S3. *Basin-averaged salinity as function of depth in the Labrador and Nordic Seas. The profiles are averaged over the last 5 years (years 46-50) of the C-Mixed (solid) and E-Greenland (dashed) experiments. Black lines are comparable profiles from the World Ocean Atlas 2009 [Antonov et al., 2010].*

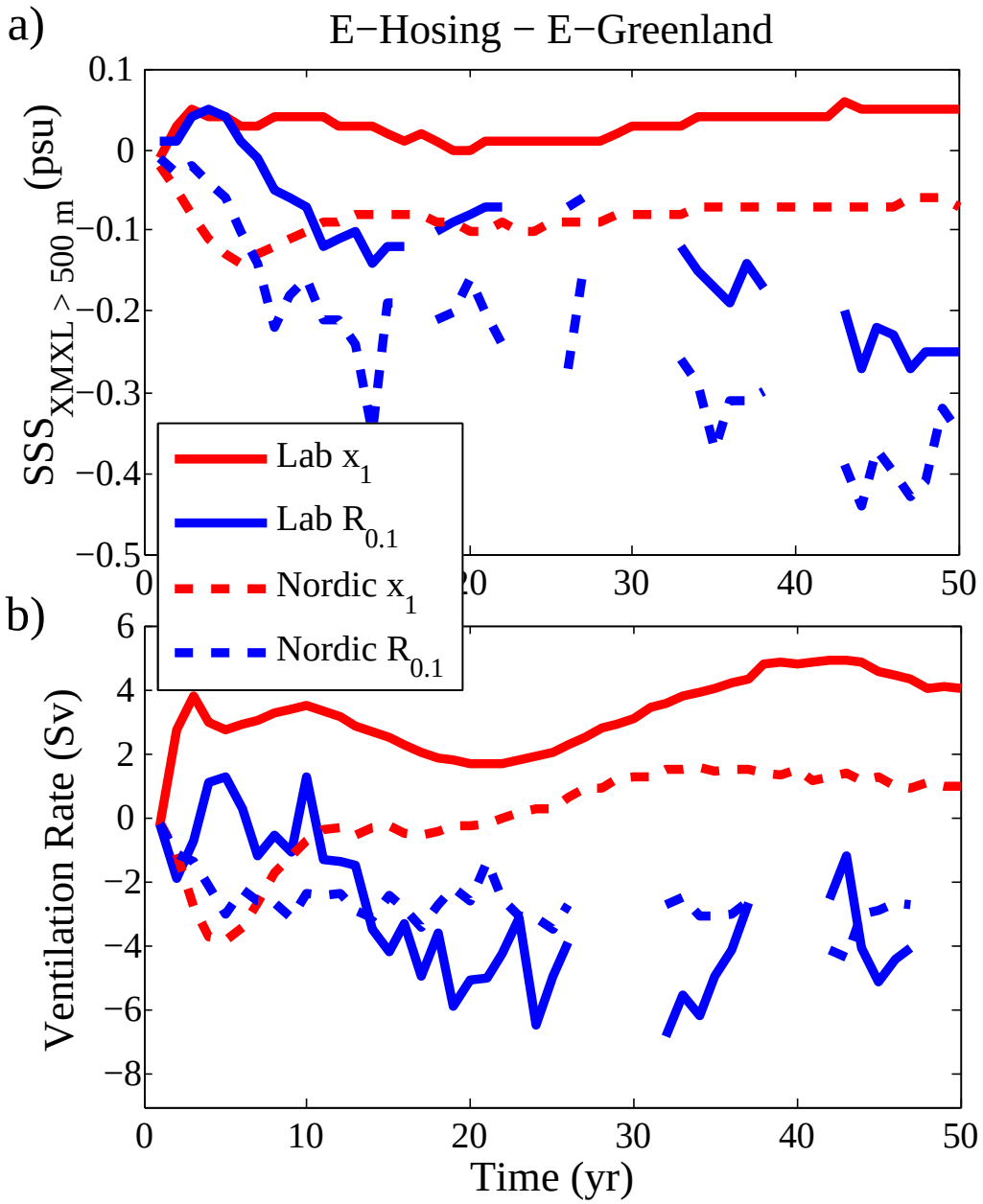

Figure S4. *a) Difference in annual-mean SSS between the E-Hosing and E-Greenland runs, for the climatological convection areas of the Labrador and Nordic Seas. The SSS are averaged over those areas where the March maximum mixed layer depth exceeds 500 m in each of these basins, averaged over the first 5 years of the C-Mixed experiments. b) Difference in ventilation rates between the E-Hosing and E-Greenland runs, for the Labrador and Nordic Seas.*